A Numerical Model for Calculation of the Restitution Coefficient of Elastic-Perfectly Plastic and Adhesive Bodies with Rough Surfaces

Ali Ghanbarzadeh[1], Ali Hassanpour[2], Anne Neville[1]

[1] School of Mechanical Engineering, University of Leeds, Leeds, UK

[2] School of Chemical and Process Engineering, University of Leeds, UK

Corresponding author: Ali Hassanpour (A.Hassanpour@leeds.ac.uk) +44(0)113 343 2405

Abstract

An in-house contact mechanics model is used to simulate contact of rough spheres having elastic-perfectly plastic contact with adhesion. The model uses a Boundary Element Method (BEM) and employs Fast Fourier Transforms (FFT) for numerical efficiency. We have validated our model for smooth surfaces with the Hertz contact behaviour in elastic regime, JKR adhesive model in the adhesive regime and Thornton and Ning's analytical model in elasto-plastic adhesive regime. Furthermore, the effect of yield stress, interface energy and surface roughness on the Coefficient of Restitution (COR) is investigated. The results show that surface roughness dramatically affects the COR and higher roughness values lead to lower CORs in general. In addition, changes of COR based on different maximum indentation depth in the presence of surface roughness consists of 3 stages; The asperity dominant, bulk elastic dominant and bulk plastic dominant. Interestingly, it was shown that there is a critical indentation depth in which the effect of surface roughness will disappear and rough surfaces act like smooth ones. This critical indentation depth is proportional to the R_q value of the surface roughness. Numerical results suggest that the yield stress influences the COR and higher yields stress results in higher COR for both rough and smooth surfaces. Results also suggest that the effect of interface energy on the COR for smooth surfaces is significant at low indentations and minimum for rough surfaces.

Keywords: Coefficient of restitution; Roughness; Adhesion; Contact mechanics

1 Introduction

Interaction of particles is an important phenomena in the assemblies of particles and their bulk behaviour in a wide range of applications such as food and biosystems [1], pharmaceuticals [2], rock mechanics [3] and gas particle flows [4]. The collision between particles have been extensively studied analytically [4], numerically [5] and experimentally [6]. In terms of the elastic contact, Hertzian contact model has been widely used which offers a non-linear behaviour [7, 8]. However, in majority of the granular flow simulations simple linear model is used to increase the computational efficiency. Since different materials show complicated plastic behaviours, incorporation of a complete analytical model for elasto-plastic contact is a challenge. Therefore semi-analytical models are often used to account for the effect of plasticity in contact mechanics [9]. Other works have introduced simplified linear models using Finite Element Analysis (FEA) [10, 11]. These models can be used to numerically and analytically calculate the COR based on the loading and unloading energy.

It was shown that adhesion is playing an important role in the dissipation of the contact energy and the coefficient of restitution and several theories were introduced [12]. In an analytical model developed by Thornton and Ning [4] coefficient of restitution was modelled for an elasto-plastic contact with consideration of adhesion. The model showed that coefficient of restitution is dependent on the impact velocity, yield stress and the interface energy. Analytical and semi-analytical models are easy to implement numerically, however they do are not able to take into account the complexities that real engineering surfaces could have such as surface roughness. The effect of surface roughness in the contact mechanics have been the subject of many studies. The pioneering work of Greenwood and Williamson (GW) [13] has shown that the surface roughness can influence the real area of contact and the discrete contact pressures. The theory assumed a distribution of the surface asperity height with similar geometry and asperity radius and the interaction of individual asperities was ignored in the model. Following that, numerous works have considered the effect of surface roughness in solving the contact problems [14-16]. Others used half-space approximation and numerous mathematical models for increasing the efficiency of the computations [17-19]. More recently, researchers developed models for the elasto-plastic contact of rough surface [20-22]. Recent advances in computational power and contact algorithms led to development of contact mechanics models with finer grids and consideration of adhesive problems [23-25]. Surface roughness is known to alter the loading and unloading behaviour of materials, therefore affecting the energy dissipation. It also dramatically affects the separation of surfaces, real area of contact and adhesion. Hence, importance of the surface roughness in calculation of energy dissipation and restitution coefficient is clear.

Despite the fast improvements in simulating the contact mechanics of real engineering surfaces, to the best of authors' knowledge, very scarce numerical models of granular materials consider the roughness as an input parameter. Recently attempts have been made to consider the effect of roughness on the normal force-displacement of particulate solids [26-28]. However, the effect of surface roughness on calculation of COR is still not studied numerically. Interestingly, this has only been studied experimentally to investigate the effect of roughness on wettability and COR in butterfly wings [29]. In this paper, a numerical in-house BEM contact mechanics model that considers elastic-perfectly plastic and adhesive contact of rough surfaces have been employed to calculate the COR. The theory of the model as well as its validation have been presented in Section 2. The effect of surface roughness, yield stress and interface energy (to take account of adhesion) on the COR has been reported in Section **Error! Reference source not found.**. The results of the current model, for the first time, highlight the importance of surface roughness in determining the COR in particle-particle interactions.

2 Theory

2.1 Elastic-perfectly plastic contact

The normal force-displacement relationship for the contact of rough particles is modelled using our contact mechanics in-house code [30]. In the case of contact of rough surfaces, only highest asperities of surfaces will stand the load and the area of real contact is orders of magnitude smaller than the nominal contact area. The contact mechanics model is a coupled model in which load on any asperity can deform the whole material with respect to the influence coefficients [7]. The problem is to solve the complementary potential energy in order to obtain the true stress and strain matrices. The composite deformation of the surfaces $u(x, y)$ due to the applied load of $p(x, y)$ can be calculated by the linear convolution according Boussinesq-Cerruti theory:

$$u_e = K * p_d = \int_{-\infty}^{+\infty} \int_{-\infty}^{+\infty} K(x - \xi, y - \eta)\, p(\xi, \eta)\, d\xi\, d\eta \tag{1}$$

in which x and y are two dimensional coordinates, K is the convolution kernel and can be calculated from the half-space approximation as the following:

$$K(x - \xi, y - \eta) = \frac{1}{\pi E^*} \frac{1}{\sqrt{(x - \xi)^2 + (y - \eta)^2}} \tag{2}$$

where E^* is the composite elastic modulus of both materials ($\frac{1}{E^*} = \frac{(1-\nu_1{}^2)}{E_1} + \frac{(1-\nu_2{}^2)}{E_2}$). Here, ν_1, ν_2, E_1 and E_2 are the Poisson's ratio and Elastic Modulus of material 1 and 2 respectively. For the sake of numerical calculations efficiency, roughness of both surfaces can be integrated as a composite surface roughness only on one contacting surface and the counter-body can be assumed to be rigid [7]. Therefore, by movement of the rigid body in normal direction, the body interferences (i) are calculated as shown in Figure 1. For the points of contact, the elastic deformation calculated using Equation 1 should be equal to the body interference (i). In order to solve the contact problem numerically, the load balance also should be considered. This will imply that the sum of all nodal contact pressures should equate the total normal applied load. The model considers a perfectly plastic behaviour and a yield criteria is assumed to be the cut-off value for the contact pressure at every node. The surface asperities that reach the yield pressure are assumed to float freely on the surface and do not take part in the deformation calculations. Therefore, the set of the following equations should be solved iteratively.

$$\left\{\begin{array}{lll} r = \left(Z_2(x,y) - Z_1(x,y)\right) + \overline{u_z}(\mathrm{x},\mathrm{y}) & \forall x,y \in A_c & (3.1) \\ p(x,y) > 0 & \forall x,y \in A_c & (3.2) \\ p(x,y) < p_y & & (3.3) \\ \sum_{i,j=1}^{i,j=N} p_{i,j} = F_N & & (3.4) \end{array}\right\} \quad (3)$$

In Equation 3 r is the rigid body movement of two rough surfaces in normal direction, Z_2 and Z_1 are the surface profiles of the two rough particles and $\overline{u_z}$ is the composite elastic deformation of two materials calculated by Equation 1. F_N is the total applied load in the normal direction, p_y is the yield stress of the softer material in contact, A_c is the area of contact and N is the total number of nodes in the domain of study. In the current contact mechanics model, an elastic-perfectly plastic approach is incorporated. Yield stress of the softer material is set to be the threshold for the plastic flow and the pressure does not exceed this value. This approach is widely used in other works in order to simulate elastic-plastic contacts. More details of the contact mechanics approach can be found in Refs [31, 32].

2.2 Adhesion

The model for adhesive contact of smooth surfaces was developed by Johnson et al. [33] (JKR) where they extended the Hertzian contact to account for adhesive region. There have been numerous attempts to adapt JKR theory to different applications [34, 35]. In recent years, development of numerical models for adhesive contact of rough surfaces have been the subject of many studies [23, 36-38]. The BEM model developed by Pohrt and Popov [39, 40] was used in this work which introduced a local mesh size-dependant criteria for detachment of surface asperities in adhesion.

In the adhesive contact the first part of Equation 3 will be modified as:

$$r = \left(Z_2(x,y) - Z_1(x,y)\right) + \overline{u_z}(\mathrm{x,y}) + d \qquad (4)$$

in which d is the pulled apart distance (Figure 2) when surfaces are unloading. It should be noted that the surface stresses that only occur inside the contact region for non-adhesive contacts are positive (compressive). When the bodies keep the same contact area after compression and are pulled away for a distance d, Equation 4 will be valid. Therefore, set of Equation 3 will be solved iteratively but the first part is replaced with Equation 4. It should be noted that the adhesive forces are considered in both loading and unloading. In order to consider adhesion in loading, after each loading step, a small unloading step (d=0.1 nm) was considered. The local detachment criteria was then applied as the following [39]:

$$p_d = \sqrt{\frac{E^*\Delta\gamma}{0.473201.h}} \qquad (5)$$

$\Delta\gamma$ is the interface energy and h is the grid size. Equation 5 calculates the maximum tensile (adhesive) pressure that a node can sustain before detachment. If the tensile stress at each node exceed the p_d value, the detachment occurs and the stress will be set to zero.

2.3 Numerical discretisation

In order to solve the set of Equations 3, the numerical domain should be discretised into rectangular elements of similar size in which the contact pressure can be assumed to be constant. Equation 1 will get the discretised form given by:

$$u_{(i,j)} = K * p_d = \sum_{k=1}^{N}\sum_{l=1}^{N} K(i-k, j-l)\, p(k,l) \qquad i,j = 1,2,\ldots,N \qquad (6)$$

where $p(k,l)$ is the constant pressure acting on the element centred at (k,l). Solving Equation 6 along with Equation 3 requires an iterative process to modify the contact pressures and finding the corresponding surface deformations. This can be solved using the matrix inversion process and requires $N^2 \times N^2$ operations. Using DC-FFT algorithm widely reported in the literature [17, 41, 42] can reduce the computational demand dramatically. Equation 6 will be then converted to:

$$u_{(i,j)} = IFFT\left[\tilde{K}_{i,j}.\tilde{p}_{i,j}\right] \qquad i,j = 1,2,\ldots.,N \qquad (7)$$

where $\widetilde{K}_{i,j}$ and $\tilde{p}_{i,j}$are the Fast Fourier Transforms (FFT) of the influence coefficient and contact pressure matrices and are multiplied element-by-element. The FFT-based convolution is accompanied by periodicity errors that can be minimized by means of zero-padding contact pressure matrix (doubling the domain and putting zero pads in both x and y directions) and wrap-around [41]. It should be noted that dealing with 2-dimensional surfaces, both contact pressure and influence matrices should be expanded in both x and y directions. In order to increase the applicability and efficiency of the method, the number of nodes chosen for the numerical study should be a power of 2. The surfaces used in this study consist of 512×512 nodes of 0.25 μm size for 500 μm radius spheres.

2.4 Calculation of the COR

It should be highlighted that parameters such as impact angle and tangential loading or friction have significant impact on the energy dissipation and the COR. In this model only the normal impact of the particles has been considered. Considering other parameters such as tangential stiffness will add more complexity to the model and can be the subject of future studies. Once the contact behaviour of loading and unloading is modelled, calculation of the COR will be straightforward by simply calculating the energy of loading and unloading from the area under the curve in load-displacement graph. The formula for the calculation of COR will be as the following:

$$COR = \sqrt{\frac{W_u}{W_l}} \qquad (8)$$

In Equation 8, $W_l$is the energy of loading that is transferred to the material and $W_u$is the energy which is released from the material in the process of unloading. The calculation of $W_l$and $W_u$is shown schematically in Figure 3.

2.5 Numerical model validations

2.5.1 Hertzian contact

An example of the surfaces used in the numerical simulation is shown in Figure 4. In order to obtain the normal force-displacement curves, the upper particle (upper surface) is moved in the normal direction. The normal force (F_N) is then calculated from the contact mechanics code solving the set of Equation 3. Movement of the upper surface is adjusted by changing the value of r in Equation 3. The indentation of the particles is simulated with step-wise increase in the value of r and the corresponding normal force is recorded. The results of normal force-displacement is compared with the Hertzian model for the case of smooth particles with 500μm radius, Young's modulus of 210 GPa (resembling a typical grade of steel) and Poisson's ratio of 0.25 in Figure 5 in order to test the accuracy of the elastic numerical model prior to elasto-plastic and adhesive simulations. It should be noted that the shape of surface asperities influence the calculation of the real contact area and the corresponding surface pressures (this is still an open area of research in the field of contact mechanics [25]). Consideration of other properties of rough surfaces such as slope of the surface roughness in the calculation of surface area, energy dissipation and COR will be the subject of future developments of the model.

2.5.2 Elastic-perfectly plastic contact

The same numerical approach as the previous section has been implemented with incorporation of the yield cut-off (Equation 3.3). It is assumed that the loading occurs in elastic-perfectly plastic mode and the unloading is only elastic. The loading and unloading of particles have been simulated and the results are compared to the analytical model of Thornton and Ning [4]. The simulations were conducted for two smooth spheres of 500μm radius with elastic modulus of 210 GPa and Poisson's ratio of 0.25. The yield pressure was set to 750MPa. Numerical BEM simulations were carried out for surfaces of 125μm×125μm. BEM numerical results of Figure 6 show very good agreement with the prediction from analytical model of Thornton and Ning [4].

2.5.3 Adhesive contact

Adhesion was considered in both loading and unloading and for validation purposes, the adhesive contact was simulated for the unloading of surfaces using the theory of Pohrt et al. [39] by step-wise increasing of parameter d in Equation 4. It should be noted that the resolution in the z direction is 0.1nm in our simulations. All the simulation parameters are the same as the elastic model shown earlier (elastic modulus of 210 GPa and Poisson's ratio of 0.25). The interface energy ($\Delta\gamma$) in the range of 0.01 to 0.09 ($\frac{J}{m^2}$) is used in Section 2.5.5 of this manuscript for comparison reasons. However, in this section and other simulations, the highest value 0.09 ($\frac{J}{m^2}$) is selected to signify the effect of adhesion on the COR for both rough and smooth surfaces. The formulation of the JKR theory has been taken from [39]. The critical point that the maximum adhesive force will occur for a parabolic profile is formulated as the following:

$$F_{adh} = \frac{3}{2}\Delta\gamma\pi R \qquad (9)$$

$$a_c = \left(\frac{9\pi}{8}\frac{\Delta\gamma R^2}{E^*}\right)^{\frac{1}{3}} \qquad (10)$$

$$d_c = -\left(\frac{3\pi^2}{64}\frac{\Delta\gamma^2 R}{E^{*2}}\right)^{\frac{1}{3}} \qquad (11)$$

F_{adh} is the total normal force required to separate the surfaces, a_{crit} is critical value of the contact radius at the moment of detachment and d_c is the crucial value of the negative indentation at the time of detachment. For comparison reasons, normalized indentation ($\bar{d}$), normalized force ($\bar{F}$) and the normalized area ($\bar{a}$) are formulated as:

$$\bar{d} = 3\bar{a}^2 - 4\bar{a}^{\frac{1}{2}} \qquad (12)$$

$$\bar{F} = \bar{a}^3 - 2\bar{a}^{\frac{3}{2}} \qquad (13)$$

$$\bar{F} \approx 0.12\left(\bar{d} + 1\right)^{\frac{5}{3}} - 1 \qquad (14)$$

The results of simulation for elastic adhesive contact are plotted in Figure 7 and compared with the JKR theory, where a good agreement can be observed.

2.5.4 Effect of yield stress

Simulations were conducted at different yield stress values of 0.75 and 1.5 GPa for adhesive contact ($\Delta\gamma = 0.09\ \frac{J}{m^2}$) of two smooth spheres. All other simulation parameters (radius, Young's modulus and Poisson ratio) are kept the same as the previous section. The results are plotted in form of COR (Equation 8) as a function of indentation depth in Figure 8. In order to compare the results with the analytical model of Thornton and Ning [4], the impact velocity in their work has been converted to the indentation depth by using the energy equations:

$$\frac{1}{2}mV^2 = \int F.di \qquad (15)$$

In the energy equation above, V is the impact velocity, m is the mass of the particle, F is the total normal force and di is the incremental indentation until the maximum indentation reaches.

It can be seen that the results are following similar trends as reported by Thornton and Ning [4], where for both yield stresses the COR initially increases by the indentation and then reduces.

2.5.5 Effect of interface energy

Interface energy is known to affect the adhesive force and thus the COR. Simulations were carried out for smooth surfaces for different values of interface energy from $\Delta\gamma = 0.01(\frac{J}{m^2})\ to\ 0.09\ (\frac{J}{m^2})$, but constant yield stress of 750 MPa. The results are plotted in Figure 9 in log scale in order to make the difference clear. Results suggest that interface energy only affects the COR at small indentations where the effect of adhesion is comparable to elastic and plastic energies. The findings are in-line with the findings of Thornton et al. [4] which used higher values for the interface energy. In this paper, we have chosen a range for the interface energy that are mostly observed in the engineering applications.

3 Effect of Root Mean Square surface roughness

Calculation of the contact behaviour of the rough surfaces is carried out using the theory presented in Section 2, considering the initial digital topography input of the model. The discretisation procedure of the rough surface topography is also discussed in Section 2.3. Rough surfaces are generated incorporating the method introduced by Hu et al. [43] who used 2-D digital filters and autocorrelation functions. Fast Fourier Transforms are used for numerical efficiency. There are several parameters that can be used to characterise the topography of the surfaces such as Root Mean Square (RMS) roughness, Skewness, kurtosis etc. Incorporation of all these surface parameters in a digitised surface needs a careful characterisation of the real engineering surfaces and extracting the desired parameters as input to the surface generation models [44]. Therefore, for simplicity, generation of rough topography was carried out by only introducing the RMS roughness of the surfaces (R_q). The topography was generated off-line prior to any contact calculations and used as input for the contact solver. Surfaces used in the model are similar to the ones shown in Figure 4. The upper surface is set to be perfectly smooth and the lower surface has the composite surface roughness of both particles in contact. The contact in this condition is known to be equivalent to the real system of two rough particles. The effect of surface roughness on the COR of an elasto-plastic adhesive contact (elastic modulus of 210 GPa, yield pressure of 750MPa and Poisson's ratio of 0.25) have been studied numerically and the results are plotted against the maximum indentation depth in Figure 10.

The maximum indentation depth is the depth that loading is stopped and the spheres start to unload. Since the contact mechanics algorithms inevitably use indentation depth and numerical simulations are based on this concept, it is more convenient to use the indentation depth as the analysis factor. More importantly, it should be noted that, analysis of rough surfaces should mainly be carried out based on indentation depth since it makes it possible to compare that with the R_q of roughness surfaces. Due to the non-linear behaviour of load and indentation, correlating incident velocity and indentation -and as a result- incident velocity and surface roughness will be highly non-linear and extracting useful information in this stage of the research will be cumbersome.

All other simulation parameters are set the same as Section 2.5.2 and Section 2.5.3. For smooth surfaces, COR increases with the maximum indentation depth due to the decreased effect of interface energy. Then a decrease in the COR is observed which is a result of plastic energy dissipation. Results for the smooth case, are in good agreement with the analytical work reported by Thornton et al. [4] in terms of the trend seen. The scenario changes when surface roughness is introduced to the contact.

4 Discussion

From results in previous sections, it can be observed that surface roughness can dramatically influence the COR. There are three distinctive stages in this case. In the first stage, the COR decreases in the beginning and that is due to the initial plastic deformation of asperities. In the second stage, a general increase in the COR is observed which can be due to the reduction in the influence of surface roughness on the overall contact behaviour as the asperities flatten [28]. Finally, a gradual decrease in the COR is observed which is similar to the smooth case and can be attributed to the plastic deformation of the bulk of particle. For the case of R_q=0.1 μm and R_q=0.2 μm this final decrease is happening earlier than the case of R_q=0.5 μm and R_q=1 μm and not surprisingly they show a closer behaviour to the smooth surface. Interestingly the values of COR tend to converge to the values for smooth case at certain indentation depths as shown by the arrows in Figure 10. This new finding suggests that in the incident of the rough particles and the corresponding COR, there is a critical indentation depth (i_{cr_max}) in which the behaviour of the rough particles align with the behaviour of smooth particles. The effect of surface roughness on the COR will disappear after the critical indentation depth (i_{cr_max}). This suggest that COR -or energy dissipation in other words- are influenced by the surface roughness mainly where the compression is in the scale of surface roughness, otherwise they tend to be close to the values of smooth surfaces. We have plotted the critical indentation depth (i_{cr_max}) against normalised surface roughness values (R_q/R) where R is the radius of particles and the results are shown in Figure 11, where a linear dependency of i_{cr_max} on the R_q/R value of the surface roughness can be observed. Moreover, as the indentation gets smaller, typically less than 50nm, the COR for all roughness values follows exactly the same trend, as in this region plasticity is not dominant. Finally, COR merges to that of a smooth surface below the indentation of 8nm, regarded as the minimum critical indentation depth (i_{cr_min}), a unique number for all roundness values. This is where the indentation gets small enough so that only tip of the first asperities come into contact. The effect of different asperity lateral sizes and slope of surface roughness will be studied on this phenomena in the future works of the author.

It is useful to analyse the energy loss due to surface roughness to highlight its significance. For comparison reasons, the percentage differences between COR values in the case of smooth surface and the case of rough surfaces ((COR_{smooth} - COR_{rough})/ COR_{smooth}) have been calculated and plotted in Figure 12. The energy dissipation due to roughness can be interpreted based on the difference shown in Figure 12. The differences in COR are not quantitatively representing the energy loss, but since COR is equal to $\sqrt{\frac{W_u}{W_l}}$, higher decrease in its value means an increase in the energy loss. Rougher surfaces show higher deviation from the behaviour of smooth surfaces for longer indentation depths therefore show higher energy losses.

4.1.1 Effect of yield stress and roughness

In order to investigate the effect of yield stress on the COR for an adhesive ($\Delta\gamma = 0.09 \frac{\mathrm{J}}{\mathrm{m}^2}$) rough surface, simulations were carried out for the surface with R_q= 0.1μm for two different values of yield stress (150 MPa and 750 MPa) and the results are presented in Figure 13. Similar to the results of Section 2.5.4, it can be seen that yield stress dramatically affects the COR also for rough surfaces. In the very initial stage of indentation (less than 50nm) where the plasticity is not yet dominant the trends are similar but a clear differentiation can be observed when the plastic deformation takes place. The trend emerges to that of a smooth particle beyond the critical indentation, where plasticity undergoes to a bulk dominant stage.

4.1.2 Effect of interface energy and roughness

The effect of interface energy on the COR for smooth surfaces has been investigated and reported in Section 2.5.5. In this section, the effect on the COR for rough surfaces is presented. Computational results for COR at two different surface energies $\Delta\gamma =$

$0.01 \left(\frac{J}{m^2}\right)$ and $0.09 \left(\frac{J}{m^2}\right)$ for the rough surface with Young's modulus of 210 GPa, yield stress of 750 MPa and R_q= 0.1μm are plotted in Figure 14. Results suggest that interface energy and therefore adhesion have less effect on the loading and unloading behaviour and the corresponding COR for rough surfaces. This is in line with other works in the literature [23, 45, 46] that state, interface energy will be dramatically reduced for rough surfaces especially where roughness is significantly larger than the atomic distances due to the large separation of surface points. However, when the surfaces are smooth (Figure 9), interface energy has significant effect on the COR, but only in the regions where plasticity is not dominant.

5 Conclusions

In this work elastic-perfectly plastic and adhesive contact behaviour of surfaces has been simulated using a fast numerical Boundary Element Model (BEM). Coefficient of Restitution (COR) was calculated by considering the loading and unloading energies of smooth and rough surfaces and the following conclusions are drawn.

- It is shown that BEM is an efficient deterministic method to model the particle contact behaviour and the corresponding loading/unloading curves.
- For rough surfaces a significant dependency of COR on the surface roughness has been observed. This is the first time that surface roughness has been considered in the numerical calculation of the COR by means of BEM.
- Our results show that higher values of R_q roughness result in lower COR for the same maximum indentation. This is because higher roughness leads to a greater energy dissipation and thus lower COR. However, this behaviour changes beyond a maximum critical indentation depth (i_{cr_max}) after which COR trend is similar to that of smooth surfaces. This was argued to be where the indentation is beyond the scale of surface roughness and the contact becomes bulk-dominant.
- It is also found that, below a minimum critical indentation (i_{cr_min}), where the behaviour is mostly elastic, rough surfaces behave similar to that of smooth surfaces.
- It has been shown that for rough surfaces, the effect of yield stress on COR is significant. The lower yield stress results in lower COR, but only in the regions where the plasticity is dominant.
- Unlike smooth surfaces, interface energy slightly affects the COR of rough surfaces but in the small indentation regions where the behaviour is more elastic. Therefore, the

effect of interface energy on COR for rough surfaces is minimal, due to larger separations of surface points for rough surfaces.

Authors believe that consideration of the surface roughness in the bulk behaviour of the granular materials as well as particle-particle interactions is significantly important and will influence the future calculations. The method is fairly fast and could be used for a variety of materials and complicated surface geometries.

References

[1] J. Horabik, M. Beczek, R. Mazur, P. Parafiniuk, M. Ryżak, M. Molenda, Determination of the restitution coefficient of seeds and coefficients of visco-elastic Hertz contact models for DEM simulations, Biosystems Engineering, 161 (2017) 106-119.
[2] R. Mukherjee, C. Mao, S. Chattoraj, B. Chaudhuri, DEM based computational model to predict moisture induced cohesion in pharmaceutical powders, International journal of pharmaceutics, 536 (2018) 301-309.
[3] B. Imre, S. Räbsamen, S.M. Springman, A coefficient of restitution of rock materials, Computers & Geosciences, 34 (2008) 339-350.
[4] C. Thornton, Z. Ning, A theoretical model for the stick/bounce behaviour of adhesive, elastic-plastic spheres, Powder technology, 99 (1998) 154-162.
[5] A. Aryaei, K. Hashemnia, K. Jafarpur, Experimental and numerical study of ball size effect on restitution coefficient in low velocity impacts, International Journal of Impact Engineering, 37 (2010) 1037-1044.
[6] C. Lun, S. Savage, The effects of an impact velocity dependent coefficient of restitution on stresses developed by sheared granular materials, Acta Mechanica, 63 (1986) 15-44.
[7] K.L. Johnson, K.L. Johnson, Contact mechanics, Cambridge university press, 1987.
[8] H. Hertz, On the contact of elastic solids, J. reine angew. Math, 92 (1881) 110.
[9] R.L. Jackson, I. Green, A finite element study of elasto-plastic hemispherical contact against a rigid flat, Journal of tribology, 127 (2005) 343-354.
[10] L. Vu-Quoc, X. Zhang, An elastoplastic contact force–displacement model in the normal direction: displacement–driven version, Proceedings of the Royal Society of London A: Mathematical, Physical and Engineering Sciences, The Royal Society, 1999, pp. 4013-4044.
[11] O.R. Walton, R.L. Braun, Viscosity, granular-temperature, and stress calculations for shearing assemblies of inelastic, frictional disks, Journal of rheology, 30 (1986) 949-980.
[12] N.V. Brilliantov, N. Albers, F. Spahn, T. Pöschel, Collision dynamics of granular particles with adhesion, Physical Review E, 76 (2007) 051302.
[13] J. Greenwood, J.P. Williamson, Contact of nominally flat surfaces, Proceedings of the Royal Society of London A: Mathematical, Physical and Engineering Sciences, The Royal Society, 1966, pp. 300-319.

[14] D.J. Whitehouse, J. Archard, The properties of random surfaces of significance in their contact, Proc. R. Soc. Lond. A, 316 (1970) 97-121.
[15] A. Bush, R. Gibson, T. Thomas, The elastic contact of a rough surface, Wear, 35 (1975) 87-111.
[16] B.N. Persson, Theory of rubber friction and contact mechanics, The Journal of Chemical Physics, 115 (2001) 3840-3861.
[17] H.M. Stanley, T. Kato, An FFT-Based Method for Rough Surface Contact, Journal of tribology, 119 (1997) 481-485.
[18] B. Bhushan, Contact mechanics of rough surfaces in tribology: multiple asperity contact, Tribology Letters, 4 (1998) 1-35.
[19] I. Polonsky, L. Keer, A numerical method for solving rough contact problems based on the multi-level multi-summation and conjugate gradient techniques, Wear, 231 (1999) 206-219.
[20] L. Pei, S. Hyun, J.F. Molinari, M.O. Robbins, Finite element modeling of elasto-plastic contact between rough surfaces, Journal of the Mechanics and Physics of Solids, 53 (2005) 2385-2409.
[21] Y. Kadin, Y. Kligerman, I. Etsion, Unloading an elastic–plastic contact of rough surfaces, Journal of the Mechanics and Physics of Solids, 54 (2006) 2652-2674.
[22] Y.-F. Gao, A. Bower, Elastic–plastic contact of a rough surface with Weierstrass profile, Proceedings of the Royal Society of London A: Mathematical, Physical and Engineering Sciences, The Royal Society, 2006, pp. 319-348.
[23] S. Medina, D. Dini, A numerical model for the deterministic analysis of adhesive rough contacts down to the nano-scale, International Journal of Solids and Structures, 51 (2014) 2620-2632.
[24] G. Carbone, M. Scaraggi, U. Tartaglino, Adhesive contact of rough surfaces: comparison between numerical calculations and analytical theories, The European Physical Journal E, 30 (2009) 65.
[25] M.H. Müser, W.B. Dapp, R. Bugnicourt, P. Sainsot, N. Lesaffre, T.A. Lubrecht, B.N. Persson, K. Harris, A. Bennett, K. Schulze, Meeting the contact-mechanics challenge, Tribology Letters, 65 (2017) 118.
[26] C.S. Sandeep, K. Senetakis, Effect of Young's Modulus and Surface Roughness on the Inter-Particle Friction of Granular Materials, Materials, 11 (2018) 217.
[27] M. Otsubo, C. O'Sullivan, Experimental and DEM assessment of the stress-dependency of surface roughness effects on shear modulus, Soils and Foundations, (2018).
[28] M. Otsubo, C. O'Sullivan, K.J. Hanley, W.W. Sim, The influence of particle surface roughness on elastic stiffness and dynamic response, (2016).
[29] N.D. Wanasekara, V.B. Chalivendra, Role of surface roughness on wettability and coefficient of restitution in butterfly wings, Soft Matter, 7 (2011) 373-379.
[30] A. Ghanbarzadeh, M. Wilson, A. Morina, D. Dowson, A. Neville, Development of a new mechano-chemical model in boundary lubrication, Tribology International, 93 (2016) 573-582.
[31] F.S. A. Almqvist, R. Larsson, S. Glavatskih, On the dry elasto-plastic contact of nominally flat surfaces, Tribology international, 40 (2007) 574-579.
[32] R.L. F Sahlin , A Almqvist, P M Lugt and P Marklund, A mixed lubrication model incorporating measured surface topography. Part 1: theory of flow factors, Proceedings of the Institution of Mechanical Engineers, Part J: Journal of Engineering Tribology, 224 (2009) 335-351.
[33] K.L. Johnson, K. Kendall, A. Roberts, Surface energy and the contact of elastic solids, Proc. R. Soc. Lond. A, 324 (1971) 301-313.
[34] Y.-S. Chu, S. Dufour, J.P. Thiery, E. Perez, F. Pincet, Johnson-Kendall-Roberts theory applied to living cells, Physical review letters, 94 (2005) 028102.
[35] D. Maugis, Extension of the Johnson-Kendall-Roberts theory of the elastic contact of spheres to large contact radii, Langmuir, 11 (1995) 679-682.
[36] L. Pastewka, M.O. Robbins, Contact between rough surfaces and a criterion for macroscopic adhesion, Proceedings of the National Academy of Sciences, (2014) 201320846.
[37] V. Rey, G. Anciaux, J.-F. Molinari, Normal adhesive contact on rough surfaces: efficient algorithm for FFT-based BEM resolution, Computational Mechanics, 60 (2017) 69-81.

[38] F. Jin, W. Zhang, Q. Wan, X. Guo, Adhesive contact of a power-law graded elastic half-space with a randomly rough rigid surface, International Journal of Solids and Structures, 81 (2016) 244-249.
[39] R. Pohrt, V.L. Popov, Adhesive contact simulation of elastic solids using local mesh-dependent detachment criterion in boundary elements method, Facta Universitatis, Series: Mechanical Engineering, 13 (2015) 3-10.
[40] V.L. Popov, R. Pohrt, Q. Li, Strength of adhesive contacts: Influence of contact geometry and material gradients, Friction, 5 (2017) 308-325.
[41] S. Liu, Q. Wang, G. Liu, A versatile method of discrete convolution and FFT (DC-FFT) for contact analyses, Wear, 243 (2000) 101-111.
[42] J.-J. Wu, Simulation of rough surfaces with FFT, Tribology international, 33 (2000) 47-58.
[43] Y. Hu, K. Tonder, Simulation of 3-D random rough surface by 2-D digital filter and Fourier analysis, International Journal of Machine Tools and Manufacture, 32 (1992) 83-90.
[44] K. Manesh, B. Ramamoorthy, M. Singaperumal, Numerical generation of anisotropic 3D non-Gaussian engineering surfaces with specified 3D surface roughness parameters, Wear, 268 (2010) 1371-1379.
[45] M. Bazrafshan, M. de Rooij, D. Schipper, On the role of adhesion and roughness in stick-slip transition at the contact of two bodies: A numerical study, Tribology international, 121 (2018) 381-388.
[46] M. Bazrafshan, M. De Rooij, M. Valefi, D. Schipper, Numerical method for the adhesive normal contact analysis based on a Dugdale approximation, Tribology international, 112 (2017) 117-128.

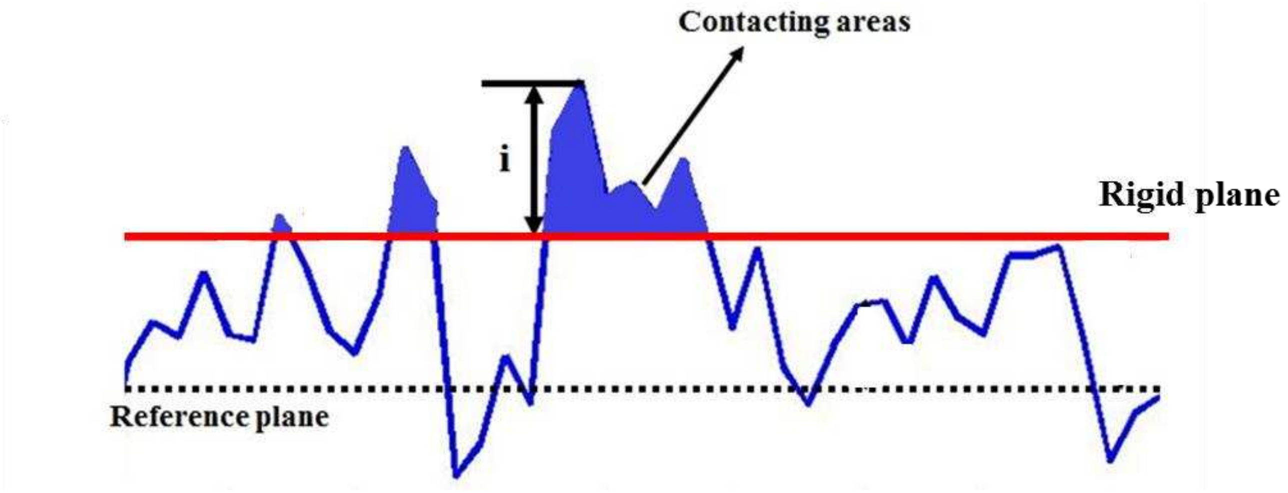

Figure 1 Schematics of the rigid body interference with the composite surface roughness

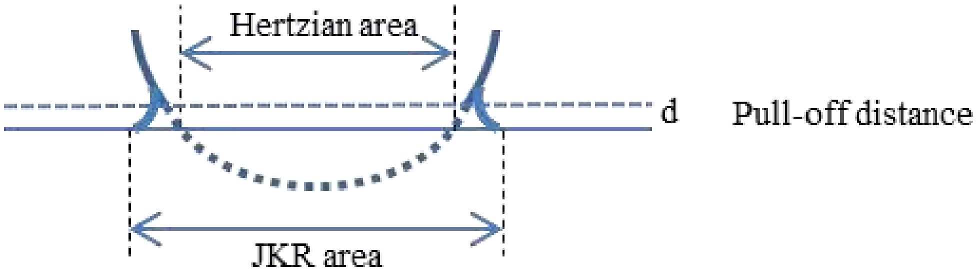

Figure 2 Illustration of the contact geometry based on JKR and Hertzian theory and the pull-off distance d. Positive (compressive) pressures occur in Hertzian region and repulsive forces are at the outer ring (JKR region). d is the distance in which surfaces are pulled apart.

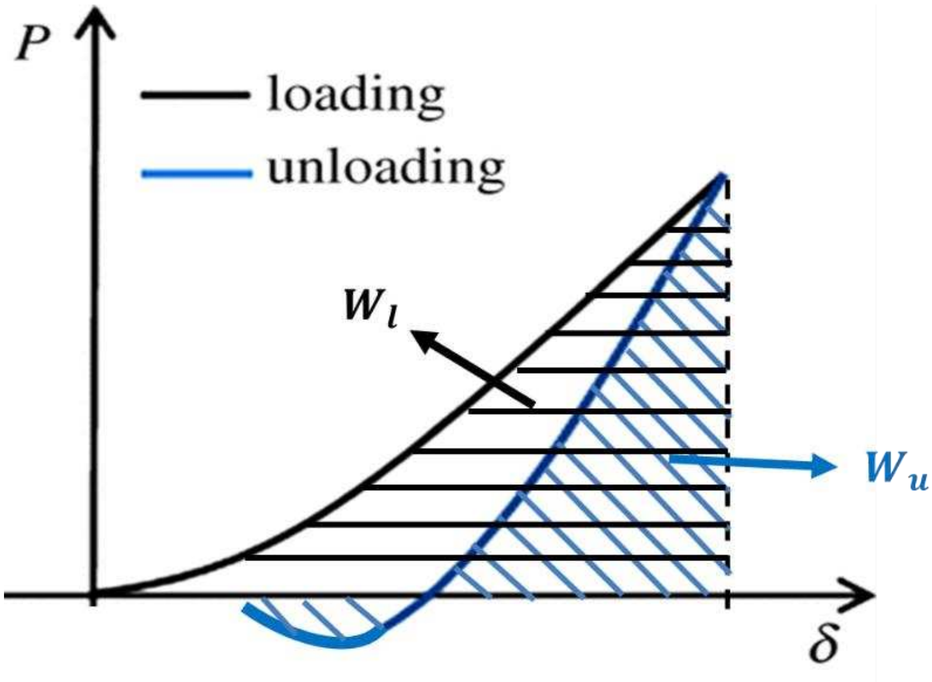

Figure 3 Schematics of loading and unloading energy calculations

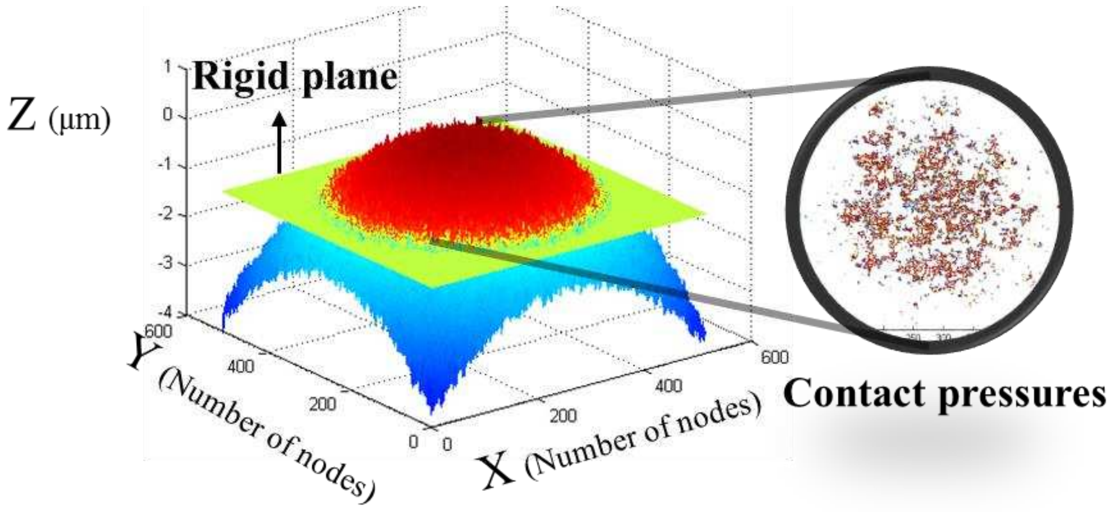

Figure 4 Digitised surfaces, domain, configuration of the BEM and the contact pressures

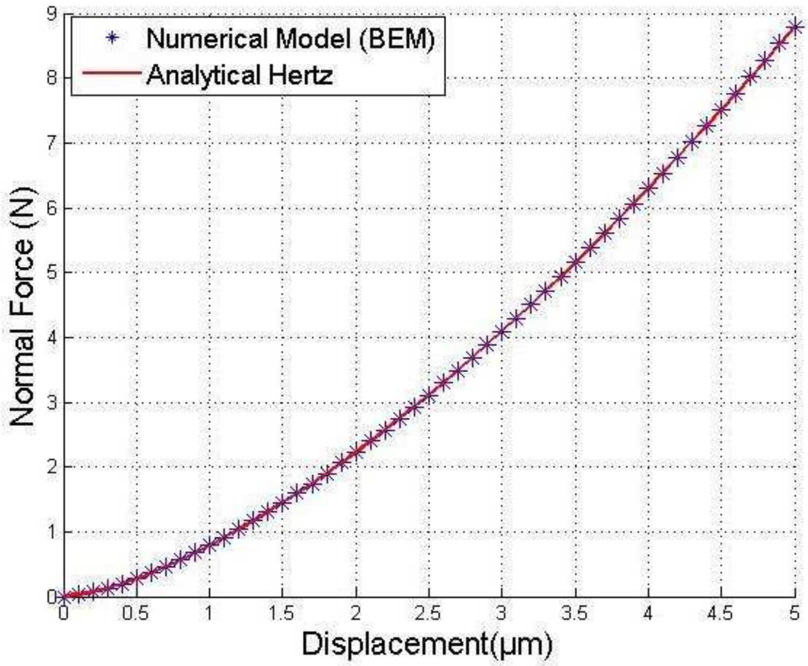

Figure 5 BEM numerical solution of the elastic contact compared with the Hertzian solution

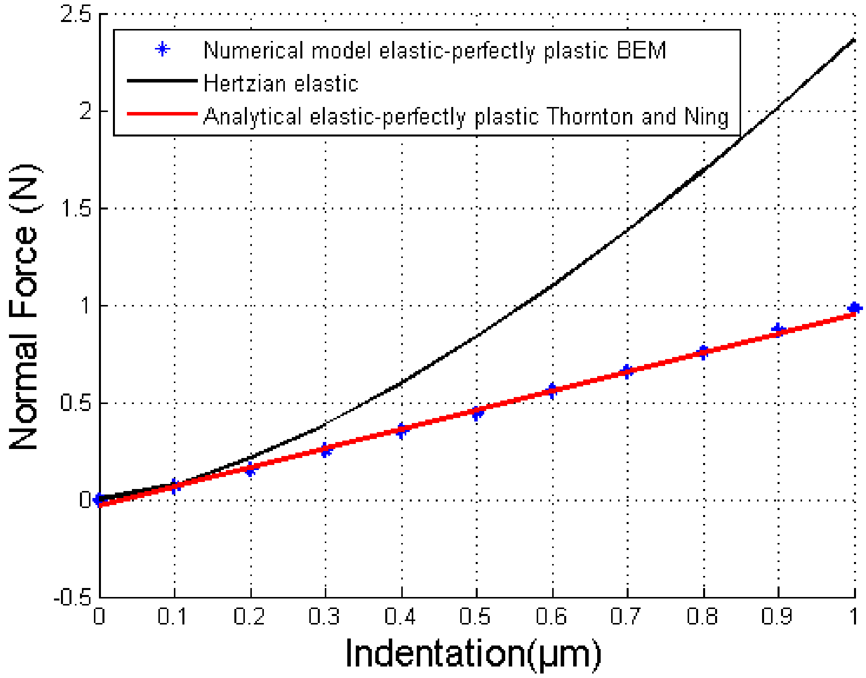

Figure 6 Comparison of different loading models

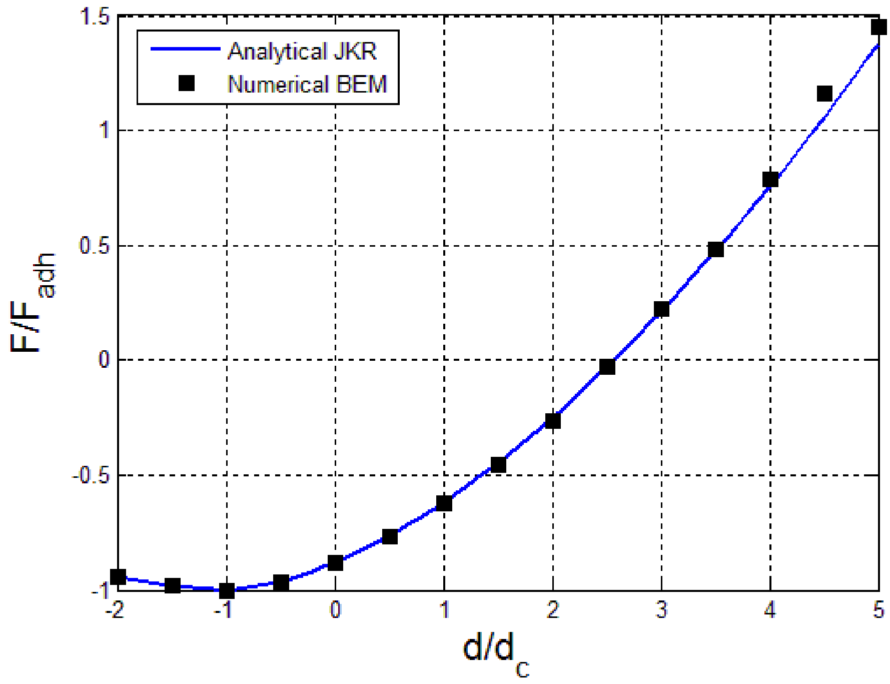

Figure 7 Adhesive pull-off for the contact of two spheres and comparison with JKR

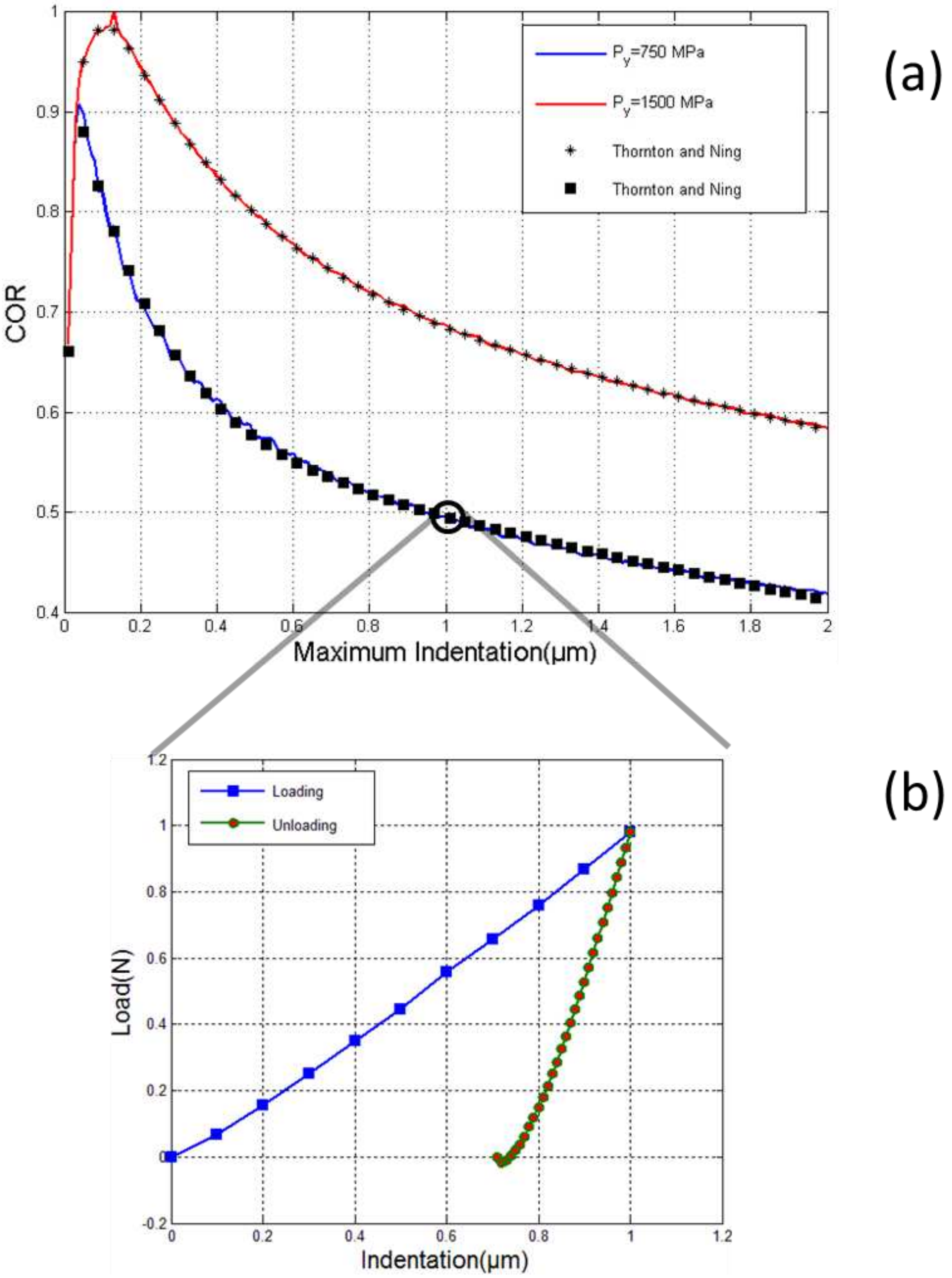

Figure 8 (a) Effect of yield stress on the COR for constant E (210 GPa) and $\Delta\gamma$ ($0.09\ \frac{J}{m^2}$) (b) one example of loading and unloading curve for elastic-perefectly plastic and adhesive contact of smooth surfaces at maximum indentation depth of 1 μm for yield stress of 750 MPa.

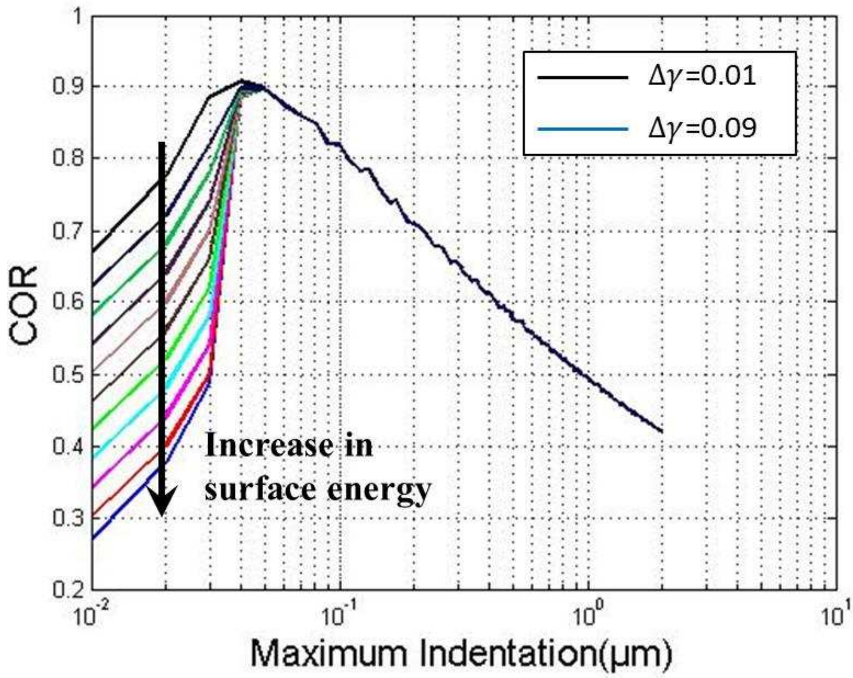

Figure 9 Effect of surface energy on the COR for $\Delta\gamma = 0.01\ to\ 0.09$ ($\frac{J}{m^2}$) but constant E (210 GPa) and yield stress (750 MPa)

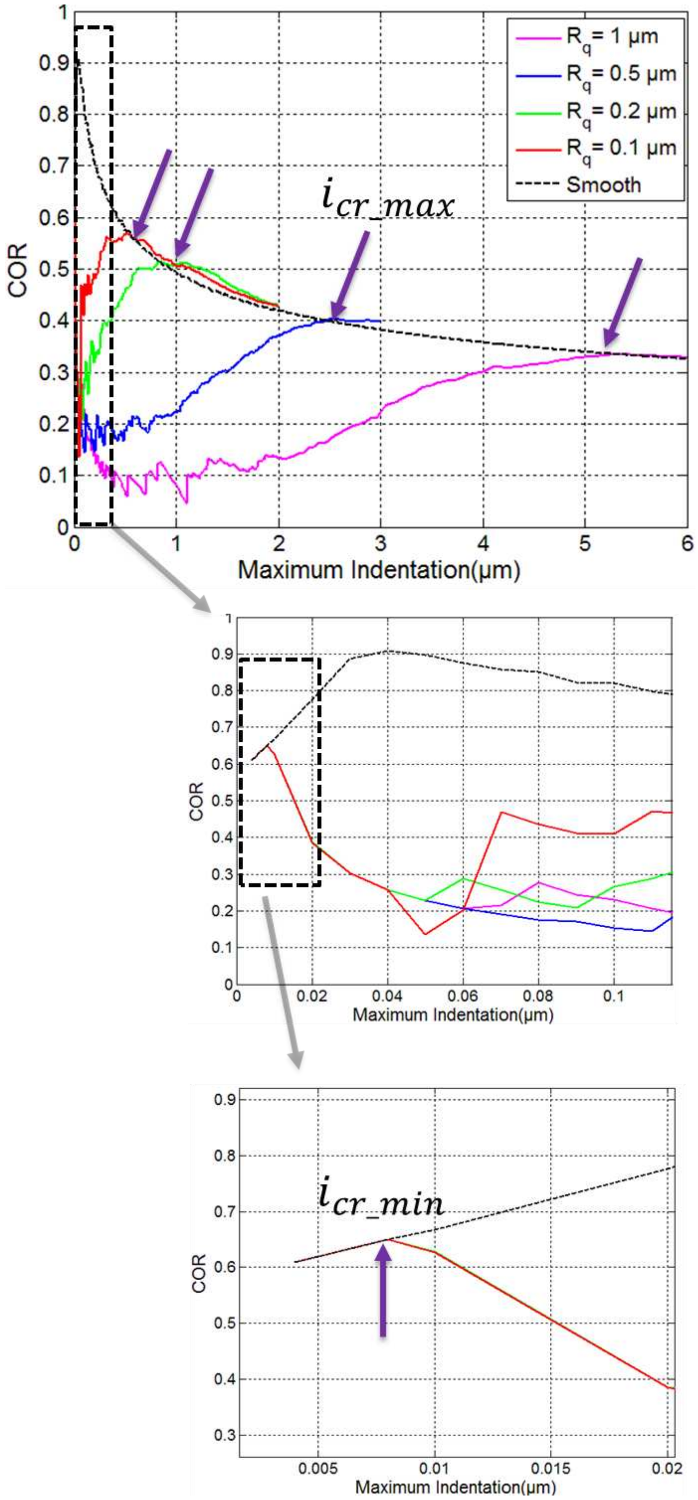

Figure 10 Effect of surface roughness on COR

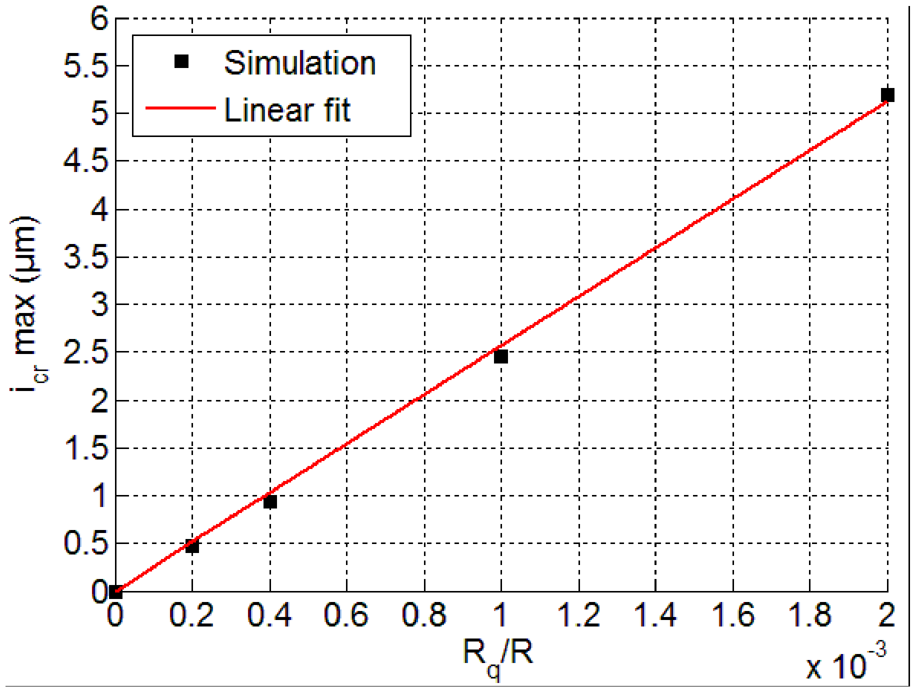

Figure 11 Critical indentation depth at different normalised roughness values

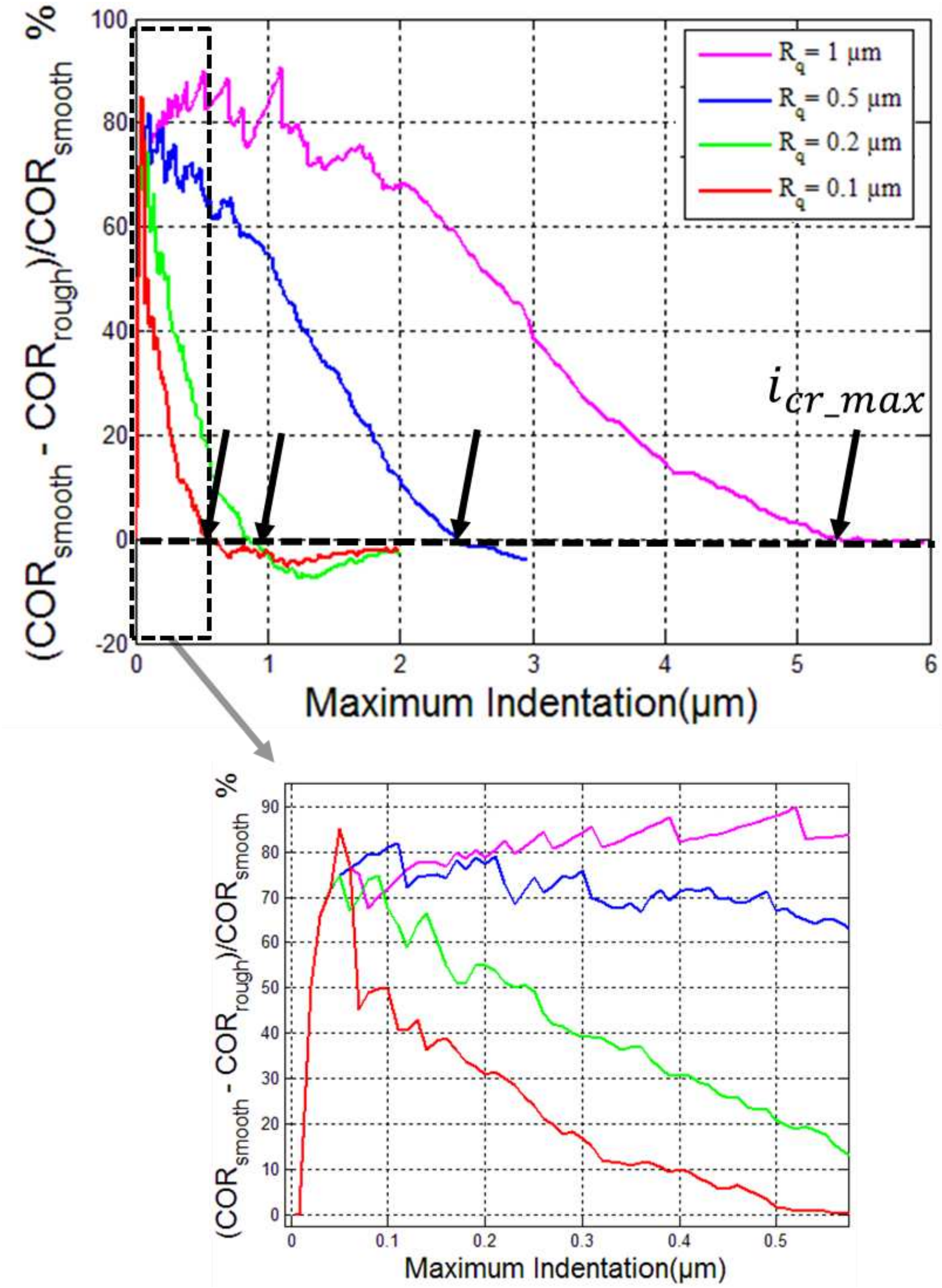

Figure 12 The difference in COR for rough and smooth surfaces.

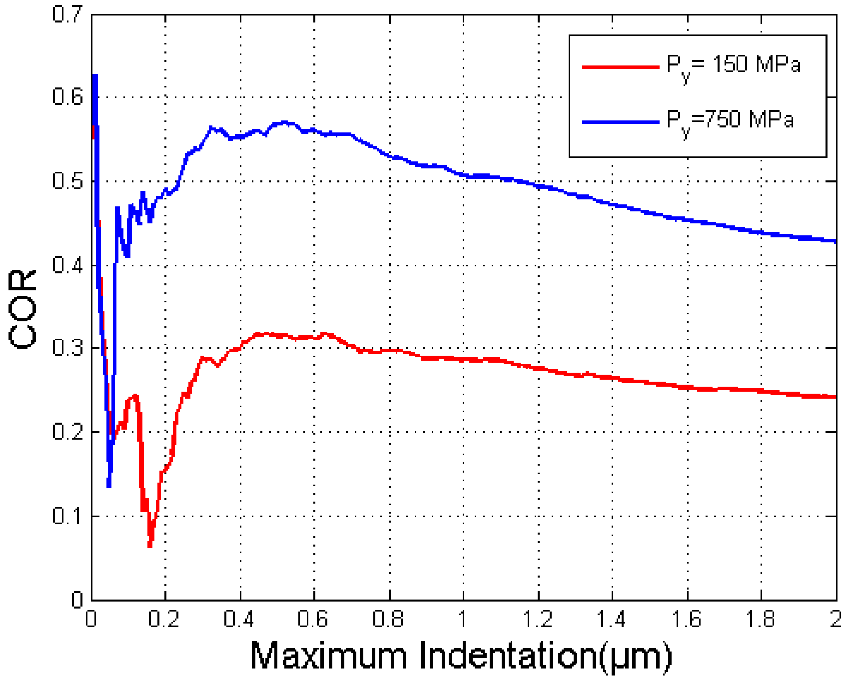

Figure 13 Effect of yield stress on the COR for rough surface with Rq= 0.1μm

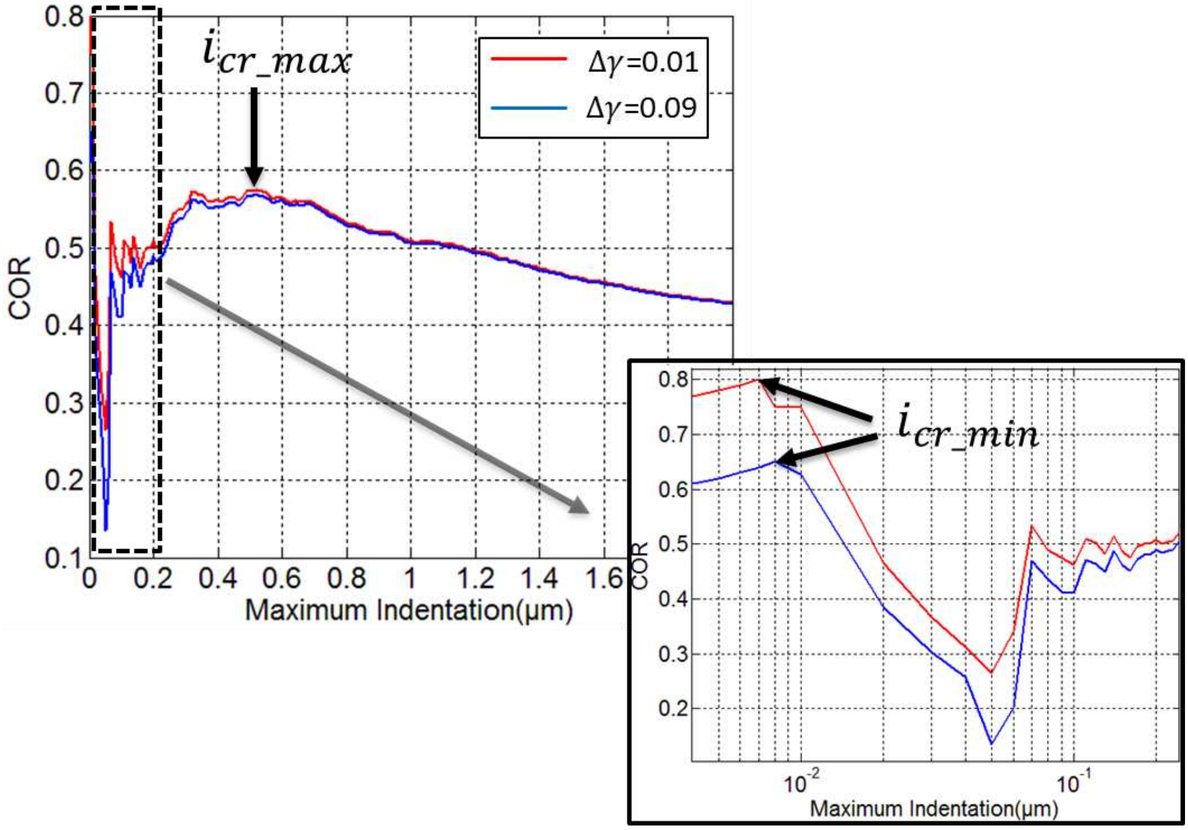

Figure 14 Effect of surface energy on the COR for rough surface with Rq= 0.1µm, E= 210 GPa and yield stress of 750 MPa